Eulerian/Lagrangian Analysis for the Prediction of Cavitation Inception

Kevin J. Farrell
Applied Research Laboratory, The Pennsylvania State University, State College, PA, USA

Abstract

An Eulerian/Lagrangian computational procedure was developed for the prediction of cavitation inception by event rate. The event rate is governed by the number distribution of nuclei, the instantaneous pressure field in the flow, the trajectory of the nuclei, and the bubble dynamics. The development of the procedure utilized an experimental database for an axisymmetric headform known as a 'Schiebe' body. The demonstration of the method in axisymmetric flows is a necessary prerequisite for application to turbomachinery flows, where the issues of grid resolution of vortices and turbulence modeling are more critical. The carrier-phase flow field was computed using an Eulerian Reynolds-Averaged Navier-Stokes solver. The Lagrangian analysis was one-way coupled to the RANS solution, since at inception, the contributions of mass, momentum, and energy of the microbubbles to the carrier flow are negligible. Probability density functions for measured nuclei populations were inverted to produce a representative population of computational bubbles, whose trajectories and growth were tracked through the flow field. The trajectories were computed using Newton's second law with models for various forces acting on the bubble. The growth was modeled using the Rayleigh-Plesset equation. The important effect of turbulence was included by adding a random velocity component to the mean flow velocity by sampling a Gaussian probability density function with variance proportional to the turbulent kinetic energy at the location of the bubble and by reducing the local static pressure by a value proportional to the turbulent kinetic energy squared. The simulation results indicate agreement with experimentally observed trends and a significant event rate at cavitation numbers above visual inception. The velocity dependence of the inception data is shown to be related to the change in the nuclei population. In this paper, the Eulerian/Lagrangian formulation is presented followed by a discussion of the simulation results of the experiment reported by Meyer, Billet, and Holl (1992).

1. Introduction

The usual approach for predicting the cavitation inception pressure for a hydraulic device is to build and evaluate a small-scale model. However, a number of similarity conditions are violated for practical reasons. The methods of properly scaling the model results to full-scale are ongoing. Most methods are based on a Reynolds number scaling to an exponent (McCormick, 1962), and vary with the cavitation type and the water quality. Any cavitation analysis requires an accurate determination of the fluid dynamics and knowledge of the bubble mechanics. The minimum pressure in a tip clearance vortex in a pump, for example, will depend on the tip clearance, flow coefficient, lift coefficient, and blade and end-wall boundary layers. While within certain restricted classes of turbomachines, the empirical scaling procedure may work satisfactorily (e. g., Farrell and Billet, 1994), a physics-based predictive capability which integrates the known variables affecting the cavitation inception problem has not been developed.

Two-phase flow can be analyzed as two fluids in the Eulerian/Eulerian approach, or as a continuum phase and a particulate phase in the Eulerian/Lagrangian or trajectory approach. The two-fluid models can easily incorporate particle diffusion effects (if data are available) and can be extended easily to multidimensional flows. However, numerical instabilities, numerical diffusion and large storage requirements for multiple particle sizes are inherent difficulties. The trajectory approach embodies the natural solution scheme for each phase and exhibits no numerical diffusion of the particulate phase. Also, storage requirements for poly-disperse particles are not excessive. Particle dispersion may be incorporated through an empirical diffusion velocity via Monte Carlo methods. A variety of models have been developed for the Eulerian/Lagrangian treatment of carrier-particle flows, and can be categorized based on the coupling between the phases, and the modeling approach.

Meyer, Billet, and Holl (1992) correlated a numerical simulation of the cavitation on a Schiebe headform with experimental inception data. A computer code was developed to statistically model cavitation inception, consisting of a numerical solution to the Rayleigh-Plesset equation coupled to a set of trajectory equations. Using the code,

trajectories and growths were computed for bubbles of varying initial sizes. An off-body distance was specified along the C_p = 0 isobar, and the bubble was free to follow an off-body trajectory. A Monte Carlo cavitation simulation was performed in which a variety of random processes, including stroboscopic observation, were modeled. Three different nuclei distributions were specified including one similar to that measured in the water tunnel experiment. The results compared favorably to the experiment. Cavitation inception was shown to be sensitive to nuclei distribution. The off-body effect was also found to be a significant factor in determining whether or not a bubble would cavitate. The traditional definition of a critical diameter based on the minimum pressure coefficient of the body or the measurement of liquid tension was found to be inadequate in defining cavitation inception. Results show that much larger bubbles are necessary because of the off-body pressure gradients which direct nuclei away from the region of minimum pressure.

Hsiao and Pauley (1999) recently completed a Reynolds-Averaged Navier-Stokes (RANS) computation of a tip vortex flow from a finite-span hydrofoil. The Rayleigh-Plesset equation for bubble growth was coupled with Johnson and Hsieh's (1966) trajectory equation to track single microbubbles through the steady-state flow field and thereby infer cavitation inception. The larger bubbles controlled the cavitation number, and their likelihood of cavitation was less dependent on the release location than for the smaller bubbles. Comparative cavitation experiments were not presented. The present work builds on this type of soft coupling, yet includes a spectrum of nuclei sizes, the effect of turbulence on trajectory and pressure, and some additional forces.

Chahine (1995) and colleagues have pursued a different approach to study the dynamics of traveling bubble cavitation inception using inviscid potential flow, but including modification of the flow by the nucleus, and allowing the nucleus to deform. Recently, the boundary element treatment of the bubble has been coupled with an unsteady RANS solution and Rayleigh-Plesset solution. These calculations have provided detailed information about the capture, growth, and collapse of a single bubble in a Rankine vortex. However, the large computation resources required to exercise these models are not required for inception nor amenable to engineering design, particularly for a large sample population of nuclei.

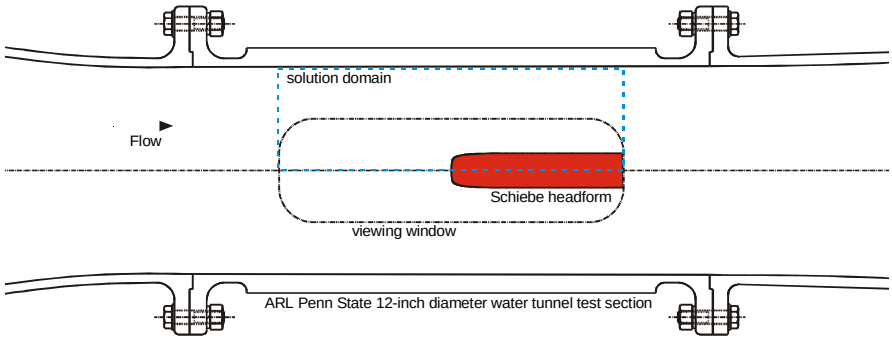

Figure 1. Schiebe headform in the ARL Penn State 12-inch Water Tunnel with solution domain.

2. Objective

The first application of this procedure was for an axisymmetric headform known as a 'Schiebe' body (Schiebe, 1972) which has been widely used for cavitation research (e. g., Gates *et al*., 1979; Hamilton, Thompson, and Billet, 1981; Holl and Carroll, 1981; Ceccio and Brennen, 1991; Meyer, Billet, and Holl, 1992; Kuhn de Chizzelle, Ceccio, and Brennen, 1995; Liu and Brennen, 1998). The headform represents a family of half-bodies formed by the addition of a disk source and a uniform stream. The headform exhibits a relatively smooth adverse pressure gradient, and the boundary layer does not separate. Because of the large database covering a number of nuclei distributions, Reynolds numbers, and geometric scales, and the well-behaved flow field, the Schiebe body is an ideal geometry for development and demonstration of the prediction method. While the eventual goal is an inception prediction capability for the vortical flows which often control the cavitation performance of many modern pump and marine propeller designs, demonstration in axisymmetric flows is a necessary prerequisite. It is important to emphasize that the technique is to be used as an engineering design tool for hydraulic devices. The micro-scales of nuclei shapes and histories are not the focus. The issue is whether or not cavitation inception is imminent in the operating range of the device. As an engineering tool, one desires an efficient procedure in order to facilitate parametric studies of design concepts and attributes, in addition to the role played by the nuclei distribution.

3. Eulerian Liquid Flow Field Analysis

The main thrust of present day computational fluid mechanics efforts at ARL Penn State for turbomachinery analysis is solutions of the RANS equations. The RANS solver employed was the incompressible UNCLE (unsteady computation of field equations) code which was developed by Professor David Whitfield and colleagues at Mississippi State University's Engineering Research Center (e.g., Taylor and Whitfield, 1991 and Whitfield, 1995). The code uses an implicit finite-volume numerical approach for solving the unsteady three-dimensional incompressible Navier-Stokes equations in a general time-dependent curvilinear coordinate system. The numerical flux at cell faces is calculated using the Roe (1981) approximate Riemann solver. Newton's method is the iterative process used to obtain both steady and unsteady solutions. The solution matrix operator is novel in that it is a discretized Jacobian, whose elements are obtained by using simple finite-differences of the flux vectors. The discretized Jacobian is then used in a combination Newton-relaxation solution method where Newton is primary and relaxation is secondary. The Navier-Stokes equations are simulated through an explicit treatment of the diffusive fluxes. Since high Reynolds numbers are of principal interest, the thin-layer approximation is applied to the transformed diffusive flux vectors. The code accommodates multiblock and dynamic grids. The UNCLE code uses artificial compressibility in order to directly couple the pressure and velocity fields and thus apply time-marching compressible flow algorithms. The code also employs the thin-layer approximation, whereby the viscous terms parallel to a vorticity generating surface are neglected as a consequence of an order-of-magnitude analysis.

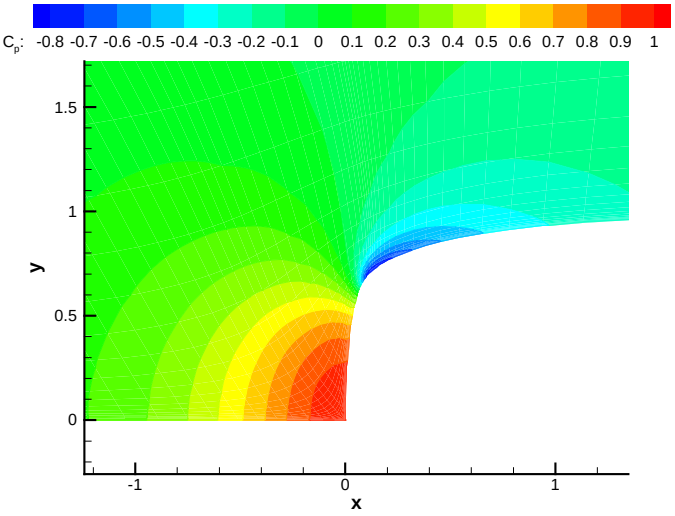

Figure 2. Computed isobars for the Schiebe headform

The solution of the Reynolds-averaged Navier-Stokes equations requires modeling of the Reynolds stress terms. In assessing the cavitation potential of a flow-field, the turbulent fluctuations of the static pressure may be important enough to cause inception in an otherwise non-cavitating flow field. On the other hand, the artificial stimulation of a boundary layer to the turbulent state may prevent cavitation. Aside from the effect on the local static pressure, the length and time scales of the carrier flow determine the dispersion of the nuclei. For these reasons, the modeling of the turbulence is very important. The original turbulence model used in the code was the Baldwin-Lomax algebraic model. Other users have subsequently added the two-equation q-ω and k-ε models (e.g., Zierke, ed., 1997). These are of particular interest here, since the turbulent kinetic energy will be used to deduce a turbulent diffusion velocity for the bubble and a turbulent pressure fluctuation which may augment bubble growth. Two-equation models are generally viewed as the minimum acceptable level of closure since the need to empirically specify either the length scale or the time scale is removed.

The specific configuration for the computational analysis is shown in Figure 1. The stagnation point on the centerline of the body is positioned at (0,0) in a Cartesian coordinate system. The coordinate values are normalized by the nominal body radius which is one inch. The domain extends 10 units upstream and 10 units downstream of the stagnation point. The outer boundary wall is nominally 6 units from the centerline, although it diverges slightly in the downstream direction. A solution was completed for a number of grids and for the Baldwin-Lomax, q-ω, and k-ε turbulence models. Grids were clustered near the solid boundaries of the Schiebe surface and the tunnel wall. The UNCLE code was actually run in three dimensions. Since the problem of interest was axisymmetric, a three-dimensional grid was achieved by rotating a planar grid one degree in the $+k$ and $-k$ directions. Thus there were three grid points and two cells in the k-direction. Periodic boundary conditions were applied to each k-face of the two-degree wedge.

The static pressure distribution over the Schiebe body is important for cavitation inception. Isobars near the stagnation point and along the shoulder past the minimum pressure point are shown in Figure 2. The sharp pressure gradient along the flat face of the headform contrasts with the sharp body normal gradient near the minimum pressure point. These features have significant consequences for cavitation inception. Near the face, the pressure gradient forces nuclei away from the body—the so-called bubble screening effect (Johnson and Hsieh, 1966). The

strong gradient near the minimum pressure point indicates that the probability of a critical nucleus entering this region is small. Thus one would expect significant scale effects, i.e. $\sigma < \left| C_{p_{\min}} \right|$. Compared to the free-field theoretical minimum pressure coefficient of -0.75, the computed value for the body in the 12-inch diameter test section was –0.78. As expected, a freefield potential solution provides a fair representation of the surface pressure distribution on the Schiebe body regardless of the flow regime model. Our purpose here is to develop a procedure with an eye to the viscous flows of turbomachinery.

4. Lagrangian Analysis of Nuclei Translation and Growth

A large volume of literature describing the motion of particles, drops, and bubbles spans over 150 years. The article of Maxey and Riley (1983) appears to be the definitive work on the subject based on the number of citations in the literature. A number of excellent review articles have appeared in the literature motivated by various multiphase flow interests: the dynamics and interactions of droplets (Sirignano, 1993), the dispersion of particles in gases and the interactions of particles with turbulence (Stock, 1996), the velocity fidelity of solid particles and bubbles used as flow tracers in optical techniques such as particle image velocimetry (PIV) (Mei, 1996), and the equation of motion and the relative importance of the various terms (Michaelides, 1997).

Maxey and Riley (1983) provided a detailed derivation of the creeping flow equation of motion, which is still considered a fairly accurate representation of the actual motion of particles. An additional consideration in the equation of motion for a bubble is its volume variation with time (Johnson and Hsieh, 1966). Collecting terms from both of these equations yields the following trajectory equation for a bubble of changing volume:

$$\frac{1}{2}\frac{4}{3}\pi a^3 \rho_f \frac{d\mathbf{V}}{dt} = -\frac{4}{3}\pi a^3 \rho_f \mathbf{g} - \frac{3}{2}\frac{4}{3}\pi a^3 \rho_f \nabla p + \frac{1}{2}\rho_f (\mathbf{U}-\mathbf{V})\left|\mathbf{U}-\mathbf{V}\right| C_D \pi a^2 + 6a^2\sqrt{\pi \rho_f \mu}\int_{t_o}^{t} \frac{\frac{d\mathbf{U}}{d\tau} - \frac{d\mathbf{V}}{d\tau}}{\sqrt{t-\tau}} d\tau + 2\pi\rho_f a^2 (\mathbf{U}-\mathbf{V})\frac{da}{dt} \qquad (1).$$

In Equation (1), the bubble mass and the Faxen terms are assumed negligible. The equation states that the product of the added mass and acceleration of the bubble is equal to the sum of the forces: buoyancy, pressure gradient, drag, history, and bubble volume variation, respectively on the right-hand side of equation (2). Other forces such as lift and Magnus forces may also be important, particularly in the complex vortical flows of turbomachinery.

An important final consideration in the motion of particles is collision dynamics. For dilute flows of interest here, the collision of particles with solid walls can be an important consideration, particularly if the minimum pressure lies on the boundary. In contrast to the assumptions of many analytical studies of the cavitating potential flows on bodies of revolution, every nucleus in a typical streamtube, which envelops a specified isobar, does not pass through that minimum pressure region—in part due to collision with the headform face. Crowe *et al.* (1998) includes an extensive discussion of particle collision models. Knowing the coefficient of restitution *e* and kinetic friction *f*, the post-collision translation and angular velocities can be obtained by solving the impulse equations subject to a number of assumptions.

The Rayleigh-Plesset equation can be derived from the continuity and momentum equations for a spherical source, which in the absence of thermal effects and assuming polytropic behavior of the gas becomes:

$$\frac{p_V - p_\infty(t)}{\rho_L} + \frac{p_{Go}}{\rho_L}\left(\frac{R_o}{R}\right)^{3k} = R\ddot{R} + \frac{3}{2}\left(\dot{R}\right)^2 + 4\frac{\nu_L}{R}\dot{R} + 2\frac{S}{\rho_L R} \qquad (2).$$

The first term of equation (2) is the instantaneous tension from the conditions far from the bubble. Equation (2) can be readily integrated to find $R(t)$ given the input $p_\infty(t)$, the initial conditions, and other constants. For initial conditions, it is usually appropriate to assume that the microbubble of radius R_o is in equilibrium at $t = 0$ in the fluid at a pressure p_∞ (0) and $dR/dt|_{t=0} = 0$. Recall that the Rayleigh-Plesset equation is based on a number of assumptions: (1) that the bubble remains spherical at all times; (2) that spatially uniform conditions exist within the bubble; (3) that no body forces such as that due to gravity are present; (4) that the density of the liquid is large and its compressibility small, compared with the values of the gas; (5) that the gas content of the bubble is constant; and (6) that the vapor pressure is the equilibrium vapor pressure.

5. Effect of Turbulence on Bubble Trajectory and Growth

Depending on a number of factors: e.g. particle size/turbulent scale ratio, the relative densities of the phase, the volume fraction of the particles, and the particle Reynolds number, the presence of a dispersed phase can augment or

attenuate the turbulence intensity (Gore and Crowe, 1989; Yarin and Hetsroni, 1994). Several models have been proposed to account for the effect of turbulence on the particle trajectories (Crowe *et al*., 1996; Yuu *et al*. (1978); Dukowics (1980); Lockwood *et al*. (1980); Jurewicz and Stock (1976); and Smith *et al.*(1981). Gosman and Ioannides' (1981) model allows a relative mean velocity between the eddy and the particles. A particle could pass through an eddy before the eddy decayed. The relative velocity between the particle and the eddy creates the *crossing trajectory effect*, which describes the supposed reduction in particle dispersion caused by a large relative mean velocity between the particles and local turbulent eddies. The simplicity and robustness of the Gosman and Ioannides (1983) model make it the primary scheme in most commercial computational codes (Crowe *et al*., 1996).

In de Jong's *et al.* (1994) analysis, turbulent diffusion is modeled by evaluating the fluid force on a particle using an instantaneous continuous phase velocity field rather than a mean velocity field. The instantaneous velocity components are obtained by adding stochastically generated turbulent velocity components to the mean velocity field for the continuous phase. The continuous phase turbulence is assumed to be isotropic, and the random turbulent velocity components are assumed to have a Gaussian probability distribution with standard deviation $\sigma = \left(\frac{2k}{3}\right)^{1/2}$ where k is the turbulent kinetic energy. The random turbulent velocity components can be obtained as $u_i = \left(\frac{4k}{3}\right)^{1/2} erf^{-1}(2x_i - 1)$ where x is a uniform random deviate. This technique is less empirical than techniques traditionally used with Eulerian-Eulerian analyses. Hinze (1975) showed that the intensity of pressure fluctuations in a homogenous isotropic flow are given by $p' = c_1 \rho k$ and that $c_1 = 0.47$ for large Reynolds numbers.

6. Numerical Procedure

A representative population of nuclei must be produced at the outset of the simulation. Nuclei populations have been measured in various bodies of water and in cavitation research tunnels. Usually the population is represented by a number distribution function *N(R)* such that the concentration of nuclei between sizes R_1 and R_2 is given by $\int_{R_1}^{R_2} N(\lambda) d\lambda$. Generally *N(R)* varies with R^{-4} or R^{-3}. For the purposes of simulation, a function is sought which maps a series of uniform deviates $\{x_1, x_2, \ldots, x_N\}$ to a set of nuclei sizes $\{y_1, y_2, \ldots, y_N\}$ distributed according to *N(R)*.

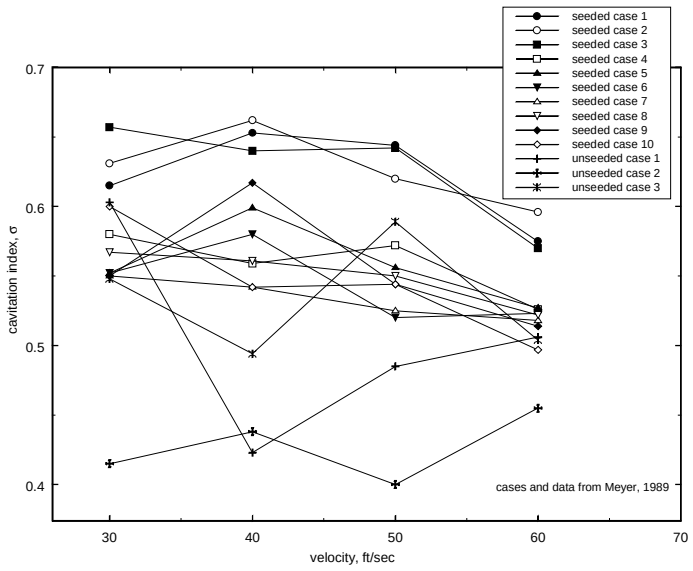

Figure 3. Visual inception data from Meyer (1989).

The values are $y(x_i) = F^{-1}(x_i)$ where the cumulative normalized probability function is $F(z) = \int_0^z p(\lambda) d\lambda$, and F^{-1} is the inverse function of F, and $p(\lambda)$ is the normalized probability distribution such that $\int_0^\infty p(\lambda) d\lambda = 1$.

Newton's second law for the motion and the Rayleigh-Plesset equation are solved for each nucleus, which is introduced randomly upstream at equilibrium. A coordinate transformation is introduced to transform the equation of motion into computational coordinate space. Grid metric quantities are evaluated in the Lagrangian code in the same manner used in the Eulerian code UNCLE. Since these metric quantities are evaluated on the cell faces, repeated interpolation was required to compute metric quantities at the location of the computational bubble, which were held constant during a single time step. Transformation between physical space and computational space is required to evaluate the bubble force terms. Once a nucleus is introduced into the flow field, various forces act upon it and determine the trajectory and hence the pressure field which will act on the nucleus. Using the local conditions along the trajectory of each nucleus, the instantaneous pressure field is computed from the mean flow and turbulence field.

If the tension is greater than the critical value for the nucleus size, then the Rayleigh-Plesset equation is solved for the new radius. A cavitation event occurs if the nucleus grows to a certain size or an acoustic emission occurs. In the current study, an event occurs when the nucleus grows to a certain size, say one millimeter, which is usually visually observable, or to ten times the original size. Once an event has occurred, the bubble is described as *cavitated* and is no longer tracked. The total rate of cavitation events can be computed based on the overall concentration of nuclei c, the nuclei release area A_c in the simulation, the mean velocity of transport for the nuclei V_c, and the probability of a cavitation event $P(e)$ according to $\dot{E} = cA_cV_c\,\mathrm{P}(e)$. The probability of a cavitation event $\mathrm{P}(e)$, the principal result of the simulation, is equal to the number of nuclei which cavitate over the number of nuclei in the ensemble.

7. Application

Meyer (1989) conducted cavitation inception tests in the ARL 12-inch diameter water tunnel with a 2-inch diameter Schiebe headform; these data are shown in Figure 3. Microbubbles were generated outside of the tunnel and seeded into the flow along the tunnel centerline upstream of the body. Microbubble sizes and populations were counted using in-line holography of a 0.45 in^3 volume at each cavitation number. Cavitation bubbles were recorded on videotape. Cavitation events, denoted by growth to 1.3 mm, were counted on the videotape and an event rate determined. The total event rate was doubled to include the flow field shadowed by the body. Cavitation inception was observed at cavitation numbers substantially lower than the absolute value of the computed minimum pressure coefficient, 0.78. A strong dependence on the nuclei spectrum is observed among the different seeded and unseeded cases. Additionally, one observes that the inception index generally declines slightly with increasing velocity, which is opposite of what one would expect for a particular nuclei spectrum, since the flux of nuclei increases with speed.

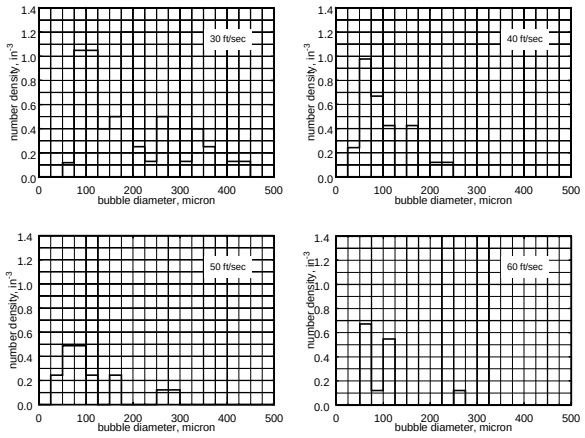

Figure 4. Measured nuclei spectra (Meyer, 1989).

Holographic images were taken during operation at the incipient cavitation index for free-stream velocities of 30, 40, 50 and 60 ft/sec. The respective number density distributions are illustrated in Figure 4. Cumulative normalized probability distributions were computed and used to generate a sample spectrum for the simulation. Figure 5 illustrates trajectories of 200 nuclei randomly placed across a portion of the inflow and shows isobars from the carrier flow. Johnson and Hsieh's (1966) screening effect is obvious for several of the microbubbles which are accelerated away from the minimum pressure area by the strong pressure gradient near the stagnation point. Several of the microbubbles cross the fluid path lines and collide with the headform. These lose momentum in the collision, and interestingly, some pass through the minimum pressure region which otherwise may not. Simulations were completed for σ = 0.5, 0.55, 0.6, 0.65, and 0.7 for free-stream velocities of 30, 40, 50, and 60 ft/sec. The cavitation event rate was

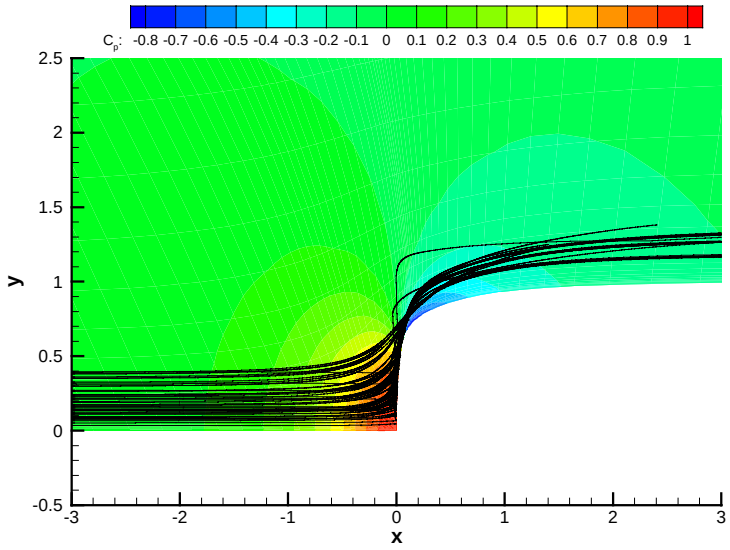

Figure 5. Simulated nuclei trajectories.

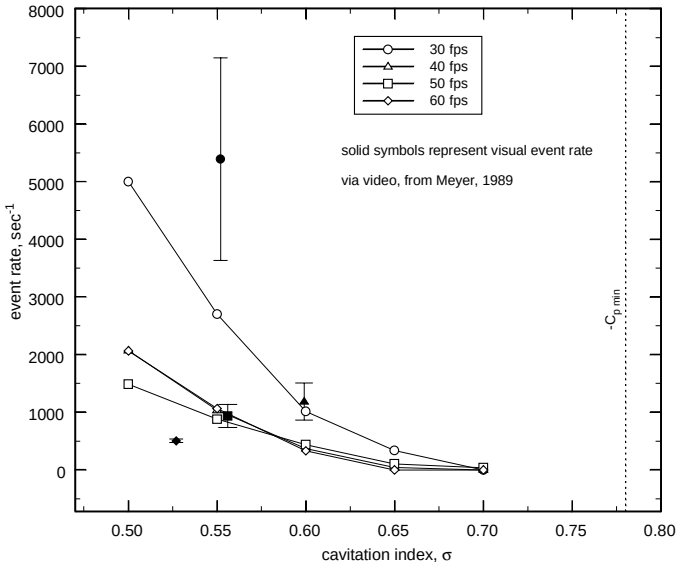

Figure 6. Simulated cavitation event rates vs. cavitation index compared to data of Meyer (1989).

computed for each case, and is plotted in Figure 6. Both the data and the simulation show a general trend of decreasing cavitation number with velocity, which is contrary to what one would expect given the increased flux of nuclei through the low pressure region with increasing speed. However, Figure 4 shows that the nuclei population decreased with increasing speed. Meyer (1989) reasoned that the experimental nuclei seeder worked less efficiently at higher speeds because the total pressure in the tunnel was lower at the lower tunnel velocities. At the higher velocities, the bubble generator was forced to pump against higher pressures, which resulted in lower flow rates of bubbles. A number of simulations were conducted with a nuclei population corresponding to the spectrum taken for 30 ft/sec in Figure 5 but for velocities of 30, 40, 50 and 60 ft/sec. The calculated event rate does increase with velocity as expected when the nuclei population is the same for all velocities.

The data of Meyer (1989) in Figure 66 show some inconsistency relative to the event rate associated with visual inception. The inconsistency arises from the fact that the event rate was determined via interrogation of the video recording, while the visual inception index was determined in real time through cavitation "calling" by eye. In Table 1, interpolated values of the cavitation number are determined for the measured event rates of Meyer (1989) and for a single representative value. The results clearly indicate the general trend of reducing cavitation number for increasing velocity.

Table 1. Comparison of Experimental and Simulated Cavitation Indices vs. Free-Stream Velocity

free-stream velocity (ft/sec)	experimental cavitation index for visual inception	Experimental event-rate via visual interrogation (sec^{-1})	predicted cavitation index at visual event rate	predicted cavitation index at 2000 events per second
30	0.55	3638-7146	0.49-0.53	0.56
40	0.60	865-1507	0.53-0.55	0.52
50	0.56	734-1132	0.59-0.61	0.50
60	0.53	537-476	0.63-0.64	0.51

8. Summary and Conclusions

An Eulerian/Lagrangian computational procedure was developed for the prediction of cavitation inception by event rate. The carrier-phase, Eulerian flow field was computed using a Reynolds-Averaged Navier-Stokes (RANS). The Lagrangian analysis was one-way coupled to the RANS solution, since at inception, the contributions of mass, momentum, and energy of the microbubbles to the carrier flow are negligible. Probability density functions for measured nuclei populations were inverted to produce a representative population of computational bubbles, whose trajectories and growth were tracked through the flow field. The trajectories were computed using Newton's second law with models for the forces acting on the microbubbles. The growth was modeled using the Rayleigh-Plesset equation. The effect of turbulence was included by adding a random velocity component to the mean flow velocity by sampling a Gaussian probability density function with variance proportional to the turbulent kinetic

energy at the location of the microbubble and by reducing the local static pressure by a value proportional to the specific turbulent kinetic energy. The simulation results indicate agreement with experimentally observed trends and a significant event rate at cavitation numbers above visual inception.

Cavitation inception data (Meyer, 1989; Kuhn de Chizelle *et al.*, 1995) show that inception indices generally decrease with increasing velocity, which is contrary to expectations based on the increased flux of nuclei to the minimum pressure region. However, nuclei populations generally are not constant for inception conditions at low and high velocities, as shown by Meyer (1989). Indeed simulations completed with Meyer's measured distributions measured at each velocity predict a reduction in cavitation number with increasing free-stream speed. At the higher static pressures associated with the increased free-stream speed, nuclei become smaller. In a more general way, this result also emphasizes the importance of an accurate microbubble number distribution; in the analyses described, all of the nuclei are assumed to be gas and not particulate.

References

Ceccio, S.L. and Brennen, C. E. (1991). *J. Fluid Mech*., **233**, 633-660.
Chaine, G. L. (1995). "Bubble Interactions with Vortices," *Fluid Vortices*, S. I. Green, ed., 783-828.
Crowe, C., Sommerfeld, M., and Tsujo, Y. (1998). *Multiphase Flows with Droplets and Particles*.
de Jong, F. J., Meyyappan, M., and Choi, S.-K. (1994). Scientific Research Associates Report R94-9085-F.
Dukowicz, J. K. (1980). *J. Comp. Phys*., **35**, 229-253.
Farrell, K. J. and Billet, M. L. (1994). *J. Fluids Eng.*, **116**, 551-557.
Gates, E. M., Billet, M. L., Katz, J., Ooi, K. K., and Holl, J. W. (1979). CalTech Rep. E244.1.
Gore, R. A. and Crowe, C. T. (1989). *Int. J. Multiphase Flow*, **15**, 279-285.
Gosman, A. D. and Ioannides, E. (1983). *J. Energy*, **7**, 482-490.
Hamilton, M. F., Thompson, D. E., and Billet, M. L. (1982*). ASME Int. Symp. on Cavitation Noise*, 25-33.
Hinze, J. O. (1975). *Turbulence*.
Holl, J. W. and Carroll, J. A. (1979). *Proceedings ASME Int. Symp. on Cavitation Inception*, 87-99.
Hsiao, C.-T. and Pauley, L. L. (1999). *J. Fluids Eng.*, **121**(1), 325-332.
Johnson, V. E., Jr. and Hsieh, T. (1966). *Sixth Naval Hydrodynamics Symposium*, 163-183.
Jurewicz, J. T. and Stock, D. E. (1976). ASME 76-WA/FE-33.
Kuhn de Chizelle, Y., Ceccio, S. L., and Brennen, C. E. (1995). *J. Fluid Mech*., **292**, 99-126.
Liu, Z. and Brennen, C. E. (1998). *J. Fluids Eng.*, **120**, 728-737.
Lockwood, F. C., Salooga, A. P., and Syed, S. A. (1980). *Combust. Flame*, **38**, 1-15.
Maxey, M. R. and Riley, J. J. (1983). *Phys. of Fluids*, **26**, 883-889.
McCormick, B. W., Jr. (1962). *J. Basic Eng*., 369-379.
Mei, R. (1996). *Exp. in Fluids*, **22**, 1-13.
Meyer, R. S., Billet, M. L., and Holl, J. W. (1992). *J. Fluids Eng.*, **114**, 672-779.
Meyer, R. S., (1989). MS thesis, Penn State Univ.
Michaelides, E. E. (1997). *J. Fluids Eng*., **119**, 233-247.
Roe, P. L. (1981). *J. Comp. Phys*., **43**, 357-372.
Schiebe, F. R. (1972). Univ. of Minnesota, St. Anthony Falls Hydraulic Lab. Rep. No. 118.
Sirignano, W. A. (1993). *J. Fluids Eng*., **115**, 345-378.
Smith, P. J., Fletcher, T. J., and Smoot, L. D. (1981). *18th Int. Symp. on Combustion*, 1285-1293.
Stock, D. E. (1996). *J. Fluids Eng*., **118**, 4-17.
Taylor, L. K. and Whitfield, D. L. (1991). AIAA Paper No. 91-1650.
Whitfield, D. L. (1995). AIAA Paper No. 95-0349.
Yarin, L. P. and Hetsroni, G. (1994). *Int. J. Multiphase Flow*, **20**, 27-44.
Yuu, S., Yasukouchi, N., Hirowawa, Y., and Jotaki, T. (1978). *A. I. Ch. E. Journal*, **24**, 509-519.
Zierke, W. C, ed. (1997). Applied Research Lab. Penn State, Rep. TR 97-002.